Application of Multiple-Model Adaptive Control Strategy for Robust Damping of Interarea Oscillations in Power System

Balarko Chaudhuri, *Student Member, IEEE*, Rajat Majumder, *Student Member, IEEE*, and Bikash C. Pal, *Senior Member, IEEE*

***Abstract*—This paper demonstrates the application of multiple-model adaptive control (MMAC) strategy for robust damping of low-frequency electromechanical oscillation in an interconnected power system. The control algorithm uses a model-based approach to account for the variability and uncertainty involved in the postdisturbance dynamics of the system. Conventional proportional-integral-derivative (PID) controllers are tuned to achieve the desired performance for each of these models. Using a Bayesian approach, the probability of each model representing the actual power system response is computed in each iteration. The resultant control action is derived as a probability-weighted average of the individual control moves of the controllers. This strategy has been used to design and test a damping controller for a thyristor controlled series compensator (TCSC) device installed in a prototype power system. The control scheme worked satisfactorily following possible disturbances without any prior knowledge about the specific postdisturbance dynamics.**

***Index Terms*—Bayesian approach, interarea oscillations, multiple-model adaptive control (MMAC), robustness, thyristor controlled series compensator (TCSC).**

I. Introduction

LOW-FREQUENCY electromechanical oscillations, involving groups of synchronous machines situated in different geographical regions, are inherent in interconnected power systems [1], [2]. These oscillations, commonly known as interarea oscillations, are characterized by lightly damped eigen values in the frequency range of 0.2–1.0 Hz. Adequate damping of these oscillations is a prerequisite for secure operation of the system. In recent times, many incidents of system outage resulting from these oscillations have been reported [1]. This has led to a renewed interest in robust damping control design to reduce the risks of system outage following undesirable oscillations.

The traditional approach for damping interarea oscillations is through installation of power system stabilizers (PSSs) [3], that provide damping control action through excitation system of the generators. In recent times, the use of controllable components in electric power transmission systems is growing gradually. These components consist of high-power electronic switches to control the current and voltage across large inductors and capacitors in different topologies. These are collectively referred to as flexible ac transmission system (FACTS) devices. Usage of these controllable components has enabled improved capacity utilization of the existing transmission lines. This avoids or, at least, delays the requirement of installing new lines which is often restricted due to economic and environmental reasons. Apart from enhancing the transfer capacity of the transmission system, supplementary control action is added to these FACTS devices to damp out interarea oscillations. In this paper, we have considered a TCSC, one of the most widely used FACTS devices in practical power systems.

The conventional damping control design approach considers a single operating condition of the system [3]. A proportional-integral (PI) or a proportional-integral-derivative (PID) controller is designed to ensure desired performance under a particular operating condition. The controllers obtained from these approaches are simple but tend to lack robustness since, at times, they fail to produce adequate damping at other operating conditions. To address this issue, researchers, over the years, have proposed several adaptive control structures for power system stabilizers. Malik *et al.* [4] applied the model reference adaptive control (MRAC) strategy where the error between the power system response and the reference model output is used to modify the controller parameters, such that the plant behavior is driven to match the behavior of the reference model. A self tuning control (STC) of PSS has been reported by Pahalawaththa *et al.* [5] where the amount of pole shifting is adjusted depending upon the system conditions. Bandyopadhayay *et al.* [6] have presented a gain scheduling control (GSC) scheme for PSS, where the controller parameters are tuned based on the minimization of the distance between the current and the desired operating points.

The main concern in power system operation is that following a disturbance (e.g., a fault in one of the buses, followed by outage of a part of the transmission network), the system switches to a different operating condition which is not known specifically in advance. From past statistics and study, one can have an approximate idea about the set of possible dynamics that are most likely to dictate the system behavior following such a disturbance. The number of elements in this set might be very high with some associated degree of uncertainty. Therefore, online identification is required to detect the trend in the

Manuscript received June 5, 2003. Manuscript received in final form February 10, 2004. Recommended by Associate Editor K. Schlacher. This work was supported by Asea Brown Boveri (ABB), USA and Engineering and Physical Science Research Council (EPSRC), England, under Grant GR/R/31676.

The authors are with the Department of Electrical and Electronic Engineering, Imperial College, London SW7 2BT, U.K. (e-mail: b.chaudhuri@imperial.ac.uk; r.majumder@imperial.ac.uk; b.pal@imperial.ac.uk).

Digital Object Identifier 10.1109/TCST.2004.833409

postdisturbance dynamic behavior and switch an appropriately weighted combination of pretuned controllers.

One such adaptive algorithm is the multiple-model adaptive controller (MMAC), which was originally introduced by Lainiotis [7]. Subsequently, it has been used for the control of aircraft [8] and for regulation of hemodynamic variables [9], [10]. Our basic motivation for applying this scheme in power system is that it can achieve the desired performance without any requirement to identify the postdisturbance dynamics prior to initiating the control action. The assumption, though, is that the actual system response can be represented by a single or a suitable combination of a finite number of linearized models. For each model, a simple PI or PID controller is designed a priori to meet the specified performance objective. Using a Bayesian approach, the current probability of each model representing the actual system response is calculated, and the results are used to determine the subsequent control moves. The probabilities are computed at every instant improving upon the probability computed from the previous instant [11]. The control move of an individual controller is assigned a weight based on the probability of that particular model representing the actual response. Thus, at each instant, the resulting control action is the probability-weighted average of the control moves of each controller.

In this paper, a damping control scheme is designed and tested for a TCSC using the MMAC approach. The TCSC is installed in a 4-machine, 11-bus prototype power system [2]. A total of 12 linearized small-signal models are required to span the entire space of anticipated responses of this system. To reduce the computation time, only five most likely models were included in control calculation. We have carried out the simulations under two scenarios. In the first case, the model governing the dominant postdisturbance dynamics was incorporated into the model bank and it was observed that the recursive algorithm could identify that particular model assigning a weight of almost one after a few initial steps. In the second case, the above model and the corresponding controller was deliberately removed from the model bank and it was found that the resultant control action involved a reasonable amount of blending between the remaining controllers depending on the probability of each model being close to the actual system response. In both the cases, interarea oscillations were found to settle satisfactorily.

II. Power System Model

The synchronous generators and their field excitation systems are the two major components of a power system that require detailed dynamic modeling for small signal stability studies. Besides generators and exciters, other components such as the dynamic loads (e.g., induction motor type), controllable devices (e.g., TCSC, PSS), prime-movers etc. require dynamic modeling as well. Different types of models have been reported in the literature for each of the above devices depending upon their specific application [3], [12]. The power flow in the network is represented by algebraic equations. This gives rise to a set of differential-algebraic equations (DAE) describing the power system behavior. This is standard modeling approach [3], [12] for interarea oscillation analysis and subsequent control synthesis. In this section, we briefly describe the governing equations for the specific types of models used in this study for each component.

A. Generator Model

The generators are represented by subtransient model with four equivalent coils on the rotor. Besides the field coil, there is one equivalent damper coil in the direct axis and two in the quadrature axis. The mechanical input power to the generator is assumed to be constant, obviating the need for modeling the prime-mover. The differential equations governing the subtransient dynamic behavior of each of the generator are given by

$$\frac{d\delta_i}{dt} = \omega_i - \omega_s \tag{1}$$

$$\frac{d\omega_i}{dt} = \frac{\omega_s}{2H}\left[T_{mi} - D(\omega_i-\omega_s) - \frac{(X''_{di}-X_{lsi})}{(X'_{di}-X_{lsi})}E'_{qi}I_{qi} - \frac{(X'_{di}-X''_{di})}{(X'_{di}-X_{lsi})}\psi_{1di}I_{qi} - \frac{(X''_{qi}-X_{lsi})}{(X'_{qi}-X_{lsi})}E'_{di}I_{di} + \frac{(X'_{qi}-X''_{qi})}{(X'_{qi}-X_{lsi})}\psi_{2qi}I_{di} + (X''_{qi}-X''_{di})I_{qi}I_{di}\right] \tag{2}$$

$$\frac{dE'_{qi}}{dt} = \frac{1}{T'_{doi}}\left[-E'_{qi} - (X_{di}-X'_{di})\left\{-I_{di} - \frac{(X'_{di}-X''_{di})}{(X'_{di}-X_{lsi})^2} \times (\psi_{1di} - (X'_{di}-X_{lsi})I_{di} - E'_{qi})\right\} + E_{fdi}\right] \tag{3}$$

$$\frac{dE'_{di}}{dt} = -\frac{1}{T'_{qoi}}\left[E'_{di} + (X_{qi}-X'_{qi})\left\{I_{qi} - \frac{(X'_{qi}-X''_{qi})}{(X'_{qi}-X_{ls})^2} \times (-\psi_{2qi} + (X'_{qi}-X_{lsi})I_{qi} - E'_{di})\right\}\right] \tag{4}$$

$$\frac{d\psi_{1di}}{dt} = \frac{1}{T''_{doi}}[-\psi_{1di} + E'_{qi} + (X'_{di}-X_{lsi})I_{di}] \tag{5}$$

$$\frac{d\psi_{2qi}}{dt} = -\frac{1}{T''_{qo}}[\psi_{2qi} + E'_{di} - (X'_{qi}-X_{lsi})I_{qi}] \tag{6}$$

for $i = 1, 2, \ldots, m$, where:

m	total number of generators;
δ_i	rotor angle;
ω_i	rotor angular speed;
E'_{qi}	transient emf due to field flux-linkage;
E'_{di}	transient emf due to flux-linkage in q axis damper coil;
ψ_{1di}	subtransient emf due to flux-linkage in d axis damper;
ψ_{2qi}	subtransient emf due to flux-linkage in q axis damper;
I_{di}	d axis component of stator current;
I_{qi}	q axis component of stator current;
$X_{di}, X'_{di}, X''_{di}$	various reactances along d axis;
$X_{qi}, X'_{qi}, X''_{qi}$	various reactances along q axis;
T'_{do}, T''_{do}	d axis open-circuit time constants;
T'_{qo}, T''_{qo}	q axis open-circuit time constants.

The stator algebraic equations are given by

$$V_i\cos(\delta_i-\theta_i) - \frac{(X''_{di}-X_{lsi})}{(X'_{di}-X_{lsi})}E'_{qi} - \frac{(X'_{di}-X''_{di})}{(X'_{di}-X_{lsi})}\psi_{1di} + R_{si}I_{qi} - X''_{di}I_{di} = 0 \tag{7}$$

$$V_i \sin(\delta_i - \theta_i) + \frac{(X''_{qi} - X_{lsi})}{(X'_{qi} - X_{lsi})} E'_{di} - \frac{(X'_{qi} - X''_{qi})}{(X'_{qi} - X_{lsi})} \psi_{2qi} - R_{si} I_{di} - X''_{qi} I_{di} = 0 \quad (8)$$

for $i = 1, 2, \ldots, m$, where:

V_i generator terminal voltage;
R_{si} resistance of the armature;
X_{lsi} armature leakage reactance.

The notation is standard and follows that in [12].

B. Exciter Model

The exciters are represented using the IEEE-DC1A type [3]. The differential equations governing their behavior are given by

$$\frac{dV_{tri}}{dt} = \frac{1}{T_{ri}}[-V_{tri} + V_{ti}] \quad (9)$$

$$\frac{dE_{fdi}}{dt} = -\frac{1}{T_{Ei}}\left[K_{Ei}E_{fdi} + E_{fdi}A_{ex}e^{B_{ex}E_{fdi}} - V_{ri}\right] \quad (10)$$

$$\frac{dV_{ri}}{dt} = \frac{1}{T_{Ai}}\left[\frac{K_{Ai}K_{Fi}}{T_{Fi}}R_{Fi} + K_{Ai}(V_{refi} - V_{tri}) - \frac{K_{Ai}K_{Fi}}{T_{Fi}}E_{fdi} - V_{ri}\right] \quad (11)$$

$$\frac{dR_{Fi}}{dt} = \frac{1}{T_{Fi}}[-R_{Fi} + E_{fdi}] \quad (12)$$

for $i = 1, 2, \ldots, m$, where:

E_{fdi} field voltage;
V_{tri} voltage measured at the generator terminal, and the rest of the notation carries their standard meaning [12].

C. Network Power Flow Model

The network power balance equations pertaining to the generator buses are given by

$$V_i \cos(\delta_i - \theta_i) I_{qi} - V_i \sin(\delta_i - \theta_i) I_{di} - S_{pi} = 0 \quad (13)$$

$$-V_i \sin(\delta_i - \theta_i) I_{qi} - V_i \cos(\delta_i - \theta_i) I_{di} - S_{qi} = 0 \quad (14)$$

where

$$S_{pi} = \sum_{k=1}^{k=n} V_i V_k [G_{ik} \cos(\theta_i - \theta_k) + B_{ik} \sin(\theta_i - \theta_k)]$$

$$S_{qi} = \sum_{k=1}^{k=n} V_i V_k [G_{ik} \sin(\theta_i - \theta_k) - B_{ik} \cos(\theta_i - \theta_k)]$$

for $i = 1, 2, \ldots, m$.

Power balance equations for the nongenerator buses are given by

$$P_{Li} + \sum_{k=1}^{k=n} V_i V_k [G_{ik} \cos(\theta_i - \theta_k) + B_{ik} \sin(\theta_i - \theta_k)] = 0 \quad (15)$$

$$Q_{Li} + \sum_{k=1}^{k=n} V_i V_k [G_{ik} \sin(\theta_i - \theta_k) - B_{ik} \cos(\theta_i - \theta_k)] = 0 \quad (16)$$

for $i = m+1, \ldots, n$, where, n is the total number of buses in the system. The equations governing the machine, exciter, network power-flow, and TCSC models were linearized about the normal operating condition to produce a linear dynamic model for eigen-analysis and control design.

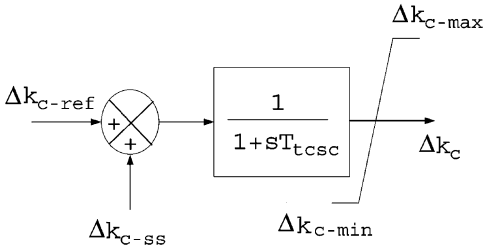

Fig. 1. Small-signal dynamic model of TCSC.

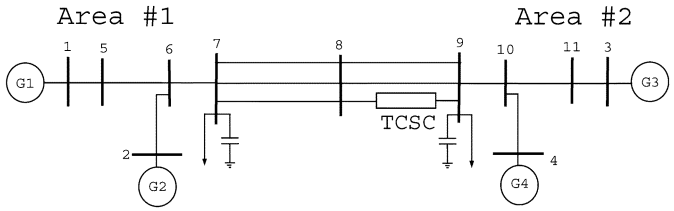

Fig. 2. Study system.

D. TCSC Model

A TCSC is a capacitive reactance compensator which consists of a series capacitor bank shunted by a thyristor controlled reactor (TCR) in order to provide a smoothly variable series capacitive reactance [13]. When the TCR firing angle is 180° , the reactor becomes nonconducting and the series capacitor has its normal impedance. As the firing angle is advanced from 180° to less than 180°, the capacitive impedance increases. At the other end, when the firing angle is 90° , the reactor become fully conducting and the TCSC helps in limiting the fault current [13]. The control over firing angle produces a variable effective capacitance, which partly compensates for the transmission line inductance and thereby, controlling the power flow through the line. The control action of the TCSC is expressed in terms of its percentage compensation k_c, defined as $k_c = (X_C)/(X_L) \times 100\%$ where X_L is the reactance of the line and X_C is the effective capacitive reactance offered by the TCSC. Continuous control over k_c enables the power flows to be changed in such a way that thermal limits are not exceeded, stability margins are increased, losses minimized, contractual requirements fulfilled, etc., without violating economic generation dispatch schedule [14]. The dynamic characteristics of a TCSC is modeled by a single time constant (T_{tcsc}) representing the response time of the TCSC control circuit as follows:

$$\frac{d}{dt}\Delta k_c = \frac{1}{T_{\text{tcsc}}}(-\Delta k_c + \Delta k_{c-\text{ref}} + \Delta k_{c-ss}). \quad (17)$$

Reference input $\Delta k_{c-\text{ref}}$, in Fig. 1, is set to a point controlling the steady-state power flow, while the supplementary input Δk_{c-ss} is controlled to damp out interarea oscillations.

III. Study System

The MMAC scheme was tested on the 4-machine, 11-bus study system, shown in Fig. 2. This system is considered as one

TABLE I
DOMINANT MODES OF OSCILLATION OF THE STUDY SYSTEM

Mode	Damping ratio	Frequency (Hz)
Inter-area	0.0129	0.6308
Local	0.0809	1.0813
Local	0.0789	1.1159

TABLE II
OPERATING CONDITIONS USED IN MODEL BANK

Model	Tie-line flow (MW)	Outage of line
1	400	No outage
2	400	7 - 8
3	400	8 - 9
4	300	No outage
5	500	No outage

of the benchmark models for performing studies on interarea oscillation because of its realistic structure and availability of system parameters [2], [3]. All the four generators are represented using subtransient model with DC (IEEE-DC1A type) exciters, as described in the previous section. The detailed dynamic data for the system can be found in [3]. The system consists of two areas connected by a weak transmission corridor. To enhance the transfer capability of the corridor, a TCSC is installed in one of the lines connecting buses #8 and #9, as shown in Fig. 2. From the transfer capacity enhancement point of view, the percentage compensation k_c of the TCSC is set to 10%. A maximum and minimum limit of 50% and %1, respectively, is imposed on the dynamic variation of k_c. Under normal operating condition, the power flow from area #1 to area #2 is 400 MW. The result of eigen value analysis for this base case, displayed in Table I, shows the presence of one lightly damped interarea mode and two local modes of oscillation [2]. Due to this lightly damped mode, there would be interarea oscillations following a disturbance in the system. The objective, therefore, is to design a damping control scheme for the TCSC to mitigate these unwanted oscillations. Moreover, the control action should be robust with respect to varying operating conditions. The real power flow in the line connecting buses #10 and #9 was chosen as the feedback stabilizing signal for the controller since the interarea mode was found to be highly observable in this measured signal.

IV. MODEL BANK

A total of 12 linearized small-signal models were required to span the entire space of anticipated response of the system following a disturbance. Disturbances include either a fault in a bus rendering outage of a line or a sudden change in power flow through the key tie-lines or a change in the nature of the loads etc. Corresponding to each of these postdisturbance operating conditions, different linearized models of the system were obtained. Ideally, each one of them should have been included in the model bank. However, to reduce computation time, only the five most probable models, in terms of their likelihood to represent the actual system response, were used. The operating scenarios and corresponding model identifiers are summarized in Table II. Model #1 is for the nominal operating condition with 400 MW power transfer through the corridor and all the tie-lines

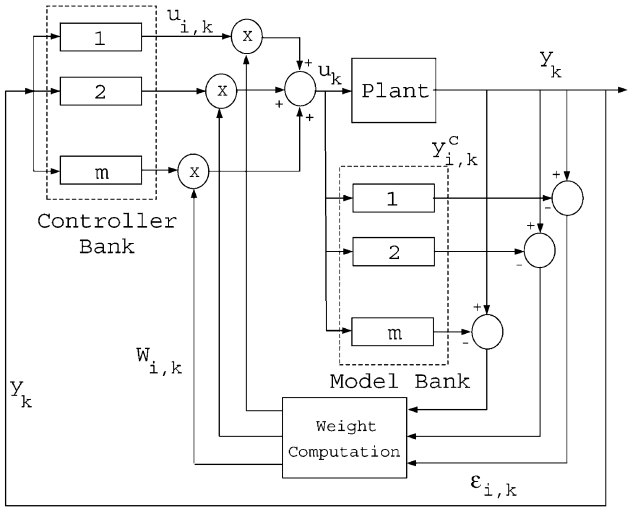

Fig. 3. Schematic of MMAC strategy.

in place. Model #2 reflects the situation with one of the tie-lines between buses #7 and #8 switched off. Model #3 corresponds to outage of one of the tie-lines connecting buses #8 and #9. In both the above cases, the tie-line power flow were assumed to remain unchanged at 400 MW. Two different tie-line power flows of 300 MW and 500 MW between area #1 and area #2 were represented by models #4 and #5, respectively, with all the tie-lines in place. Throughout the rest of the paper, the model identifiers described in Table II have been used to refer to the specific models.

V. OVERVIEW OF MMAC STRATEGY

A schematic overview of the conventional MMAC scheme is given in Fig. 3. The recursive algorithm uses a bank of linearized plant models to capture the possible system dynamics following a disturbance. One separate controller k is designed and tuned, a priori, based on each model k from the model bank. At each simulation step, the actual plant response is compared with the response of the linearized models which are driven by the same control input. The differences in the response of each model with respect to the actual system response is used to generate individual model residuals. Using these residuals, the probability of each model representing the actual system response is computed. Based on the probabilities, suitable weights are assigned to individual control moves such that the less probable models carry less weight. This ensures that the controllers designed for less probable models influence the final control move to a lesser extent. The resultant control action is, thus, a probability weighted average of the control moves of each individual controller. At each stage of the recursive algorithm, primarily two tasks are performed, i.e., calculation of probability using a Bayesian approach and assigning suitable weights based on the value of probability.

A. Calculation of Probability: Bayesian Approach

The recursive Bayes theorem is used for computing the probability of each model in the bank. The theorem calculates the conditional probability of the ith model in the model bank being the true model of the plant given this population of model. The

probabilities are assumed to be stochastic and Gaussian in nature, and thus, take a form of the exponential of the negative square of the residuals [11]. At the kth step, the probability for the ith model is calculated as

$$p_{i,k} = \frac{\exp\left(-\frac{1}{2}\varepsilon_{i,k}^T C_f \varepsilon_{i,k}\right) p_{i,k-1}}{\sum_{j=1}^{N} \exp\left(-\frac{1}{2}\varepsilon_{j,k}^T C_f \varepsilon_{j,k}\right) p_{j,k-1}} \tag{18}$$

where

$$\varepsilon_{i,k} = y_k - y_{i,k}^c \tag{19}$$

is the error or model residual at the current step. N denotes the total number of models in the model bank and C_f is the convergence factor that is used to tune the rate of convergence of the probabilities. Large values of C_f will magnify the model residuals and cause an acceleration of convergence to a single model. The recursion is initialized by assigning equal probability $(1/N)$ to all the models in the bank. At each iteration, new probabilities are calculated improving upon the probability computed at the previous iteration. One major advantage is that this algorithm is computationally inexpensive. An additional benefit is that the poor models are rejected exponentially and thereby allowing to have a widely varying set of models without necessarily leading to a large drop in controller performance, even during the initial stages [15].

To summarize, for a given set of models, the above algorithm recursively determines the probability that the ith model is the true plant model. The computation is based on the present model residuals with respect to the actual system response and the previous probabilities for each model [11].

B. Calculation of Weights

Based on the probability of individual models, calculated during each recursive step, suitable weights are assigned to the control moves of each of the controllers. The model with a higher probability is assigned a higher weight and vice versa. One of the feature of this Bayesian approach is that it can only assume a steady-state probability of either zero or one and consequently, the algorithm converges to a single model. However, due to the uncertainties associated with a practical power system, it is unlikely that any single model in the model bank would be exactly equivalent to the system under control, and hence, proper blending of control action is often required. Models attaining a probability of zero cannot enter the subsequent recursions, and hence, an artificial cutoff $\beta_{\min}$ is used to keep them alive. At the kth step, the ith model is assigned a weight $W_{i,k}$ such that

$$W_{i,k} = \begin{cases} \frac{p_{i,k}}{\sum_{j=1}^{N} p_{j,k}} & \forall p_{i,k} > \beta_{\min} \\ W_{i,k} = 0 & \forall p_{i,k} < \beta_{\min} \end{cases}. \tag{20}$$

For models with $p_{i,k} < \beta_{\min}$, the probability is reset to $p_{i,k} = \beta_{\min}$ and these models are then excluded from being weighted. At the kth iteration, the resulting probability-weighted control move is computed as

$$u_k = \sum_{j=1}^{N} W_{j,k} \cdot u_{j,k}. \tag{21}$$

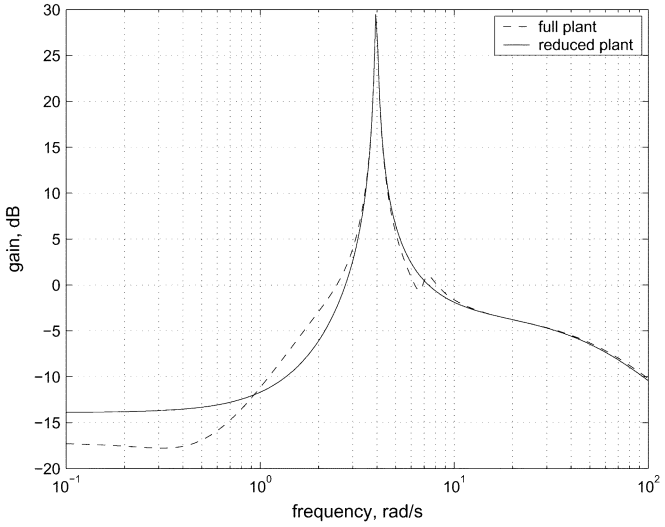

Fig. 4. Frequency response of the plant.

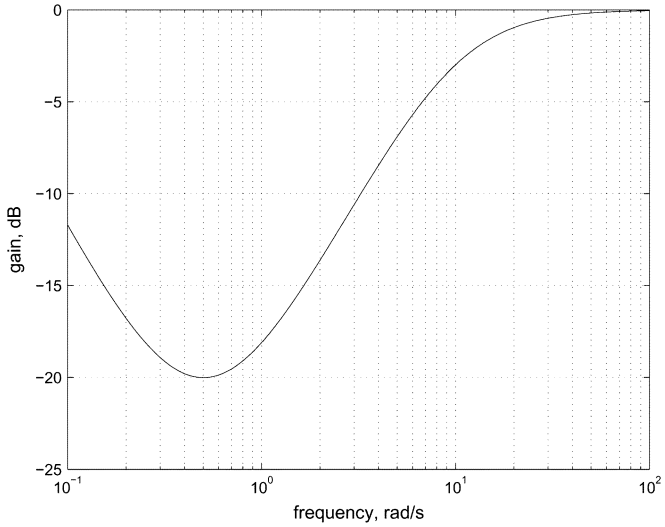

Fig. 5. Frequency response of the controller.

VI. Control Tuning and Robustness Testing

The first step toward the implementation of the MMAC scheme is to design and tune the controllers for the five linearized system models, described in Section IV. The order for each of these plant models was 41. To facilitate control design, the nominal plant was reduced to third-order equivalents without loosing much of the relevant information in the frequency range of interest (0.1–1.0 Hz), as illustrated in Fig. 4. To improve the damping ratio of the critical interarea mode, a simple PID controller, as shown in Fig. 5, was designed for the reduced plant model using the conventional gain-margin and phase margin based techniques [16]. The controller gain required additional tuning to meet the specified closed-loop performance criteria. In this case, the criterion was to achieve a closed-loop damping ratio of 0.25 for the interarea mode under all operating conditions. A damping ratio of 0.25 generally ensures, in the experience of the authors, satisfactory settling of interarea oscillations within 10 s, a criterion followed by the power system utilities [1]. The controller gains were adjusted

TABLE III
CLOSED-LOOP DAMPING RATIO OF THE INTERAREA MODE FOR DIFFERENT MODELS AND CONTROLLERS

Controller No.	Model No.				
	1	2	3	4	5
1	0.25	0.23	unstable	0.17	unstable
2	0.26	0.25	unstable	0.18	unstable
3	0.16	0.15	0.25	0.11	0.22
4	unstable	unstable	unstable	0.25	unstable
5	0.18	0.17	0.27	0.12	0.25

individually for each model, using root locus techniques to achieve a damping ratio of 0.25 for the interarea mode i.e., the controller k was tuned so as to ensure a closed-loop interarea mode damping ratio of 0.25 for model k. However, this did not necessarily ensure that satisfactory damping ratios would be preserved using controller k for models other than k. In fact, it is clear from Table III that in certain cases, either the system becomes unstable or the damping ratio is below the acceptable limit. For the cases marked as "unstable" in Table III, the damping ratio for the interarea mode was acceptable, but some of the other modes incurred negative damping ratios. If the controllers were tuned to obtain a less conservative damping ratio of 0.15 instead of 0.25, then the instabilities could be avoided in some cases, but some of the damping ratios under certain operating conditions went below 0.1, which is not acceptable for secure operation of the power system. It is to be noted that although the above discussion is specific to this particular test system, it still represents the general lack of robustness of the conventionally tuned controllers under different operating conditions encountered in a practical power system.

VII. TEST CASES

It is clear from the results shown in Table III that a conventional controller k, designed, and tuned on the basis of model k, is not necessarily guaranteed to meet the desired performance specification for other models. Therefore, some mechanism needs to be devised for online identification of the unknown dominant dynamics following a disturbance and switch to an appropriately weighted combination of the controllers. Two situations can arise considering the uncertainty involved in a practical power system and the limit on the number of models that can be included in the model bank from computational complexity point of view. In one case, the model corresponding to the dominant postdisturbance dynamics is likely to be present in the model bank, wherein, the scheme should pick up the controller corresponding to that model with maximum weight. In the other case, the model representing the dominant postdisturbance dynamics is less likely to be present in the model bank, wherein, the scheme should be able to ensure proper blending between the control moves of the existing controllers and achieve the desired performance criteria. These two test cases have been treated separately in this paper and are elaborated in the following sections.

A. Test Case I

For this test case, a three-phase-line-to-ground fault was simulated at bus #8 for 80 ms, followed by opening of one of the tie-lines connecting buses #7 and #8, see Fig. 2. From Table II, it can be seen that the dynamics corresponding to this particular postdisturbance situation is captured in model #2. All the five models, including model #2, were kept in the model bank and the corresponding controllers in the controller bank. The objective was to see whether and how quickly could the adopted MMAC algorithm identify the dominant postdisturbance dynamics and switch the appropriate controller to achieve the desired performance.

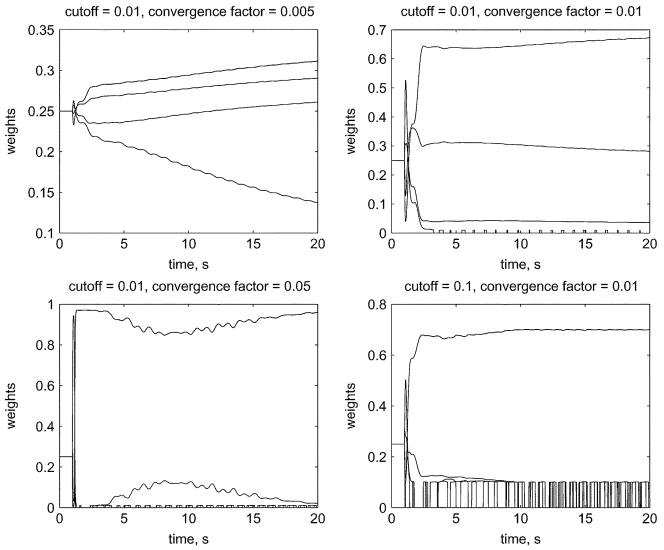

Fig. 6. Variation of the computed weights.

B. Test Case II

For this test case, the same disturbance, as described before, was considered. Due to the uncertainty involved in a practical power system, it is unlikely that any single model in the model bank would be the exact equivalent of the system under control. Moreover, due to computational constraints, only a few out of the large number of possible models can be included in the model bank. To replicate these two likely situations, model #2 and the corresponding controller #2 were deliberately removed from the respective banks. The idea was to validate whether a blended version of the remaining control moves is able to achieve the desired performance in the absence of the actual controller. This would demonstrate the ability of the MMAC algorithm to pick up a proper blend of the relevant postdisturbance dynamics to closely mimic the actual system response.

VIII. CHOICE OF CONVERGENCE FACTOR AND ARTIFICIAL CUTOFF

Two of the most important factors influencing the success of a MMAC scheme are the proper choice of the convergence factor C_f and the artificial cutoff $\beta_{\min}$, described in (18) and (20), respectively. The choice, of course, is very much dependent on the specific system to be controlled and the design of the model banks. Although there are no hard and fast rules for choosing these parameters, a general guideline can be presented. Fig. 6 shows the variation of the computed weights with time for some selected values of C_f and $\beta_{\min}$. It can be seen that with increasing value of C_f, the poor models are rejected quickly,

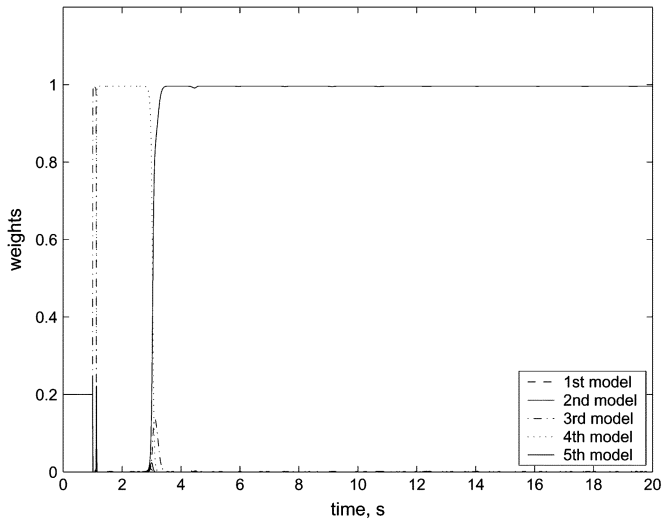

Fig. 7. Test case I. Variation of the weights corresponding to each model.

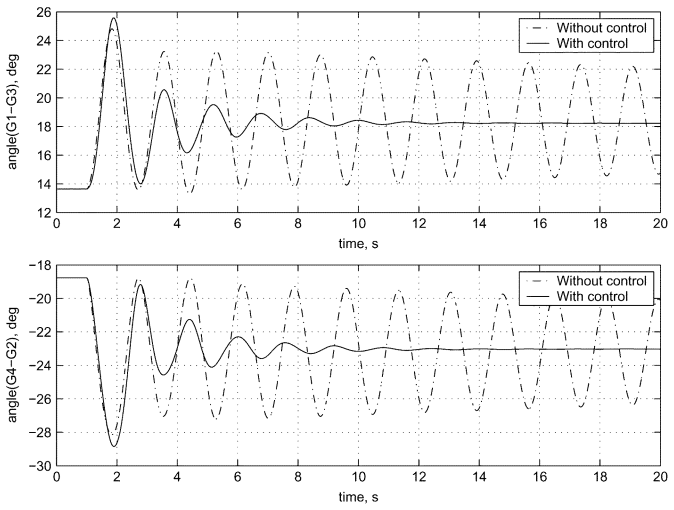

Fig. 8. Test case I. Dynamic response of the system.

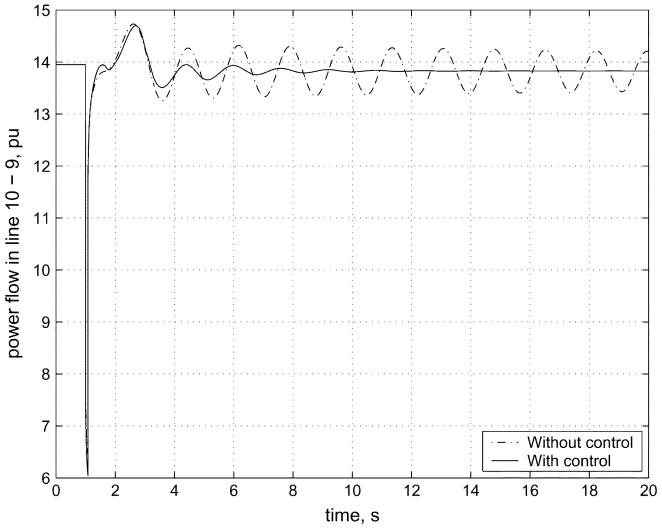

Fig. 9. Test case I. Power flow between buses #10 and #9.

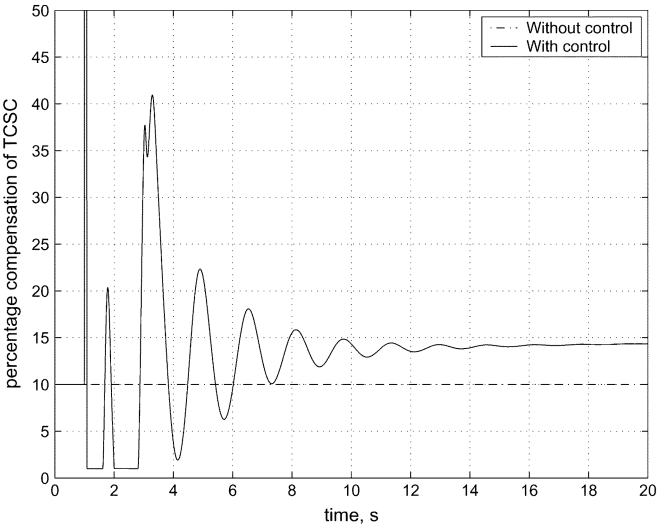

Fig. 10. Test case I. Response of the controller.

whereas lower values of C_f help blending. Higher values of the cutoff $\beta_{\min}$, on the other hand, retain even the least probable models to help blending. If there is a high chance that the postdisturbance behavior would be dominated by one of the models in the model bank, then it is preferable to use a high value of C_f to quickly reject the unwanted models and a low value of $\beta_{\min}$ to prevent them from being retained during recursion. For a practical power system, this might not always be the relevant scenario. In practice, the number of probable models is too large for them all to be included in the model bank, avoiding the computational constraints. Moreover, due to the uncertainties involved in the parameters, it is unlikely that any single model in the model bank would be exactly equivalent to the system under control. The calculated values of model residuals during the initial stages might be misleading in the sense that the dynamics of the system during the fault is often completely different from that during the postfault situation. Therefore, instead of quickly rejecting the majority of the models based on the initial model residuals, blending is preferred by using lower values of C_f and higher values of $\beta_{\min}$.

IX. Simulation Results

The simulations were performed in the *Simulink* environment of *Matlab* using a step-size of 1 ms and fourth–order Runge–Kutta solver. The results are separately presented for the two test cases.

A. Test Case I

The results of the time domain simulation for test case I are shown in Figs. 7–10. Here, the linearized model of the power system corresponding to the postdisturbance situation (model #2) was considered to be present in the model bank. As a result, the residual for model #2 starts decreasing after few initial recursive steps and consequently the weight corresponding to this model goes up and attain a steady-state value of almost one, see Fig. 7. Our objective, in this case, is to demonstrate the ability of the MMAC scheme to identify the unknown dynamics and switch to the proper controller. This is why a relatively high magnitude of 0.05 is chosen for the convergence factor C_f to quickly reject the unwanted models. Also, the ar-

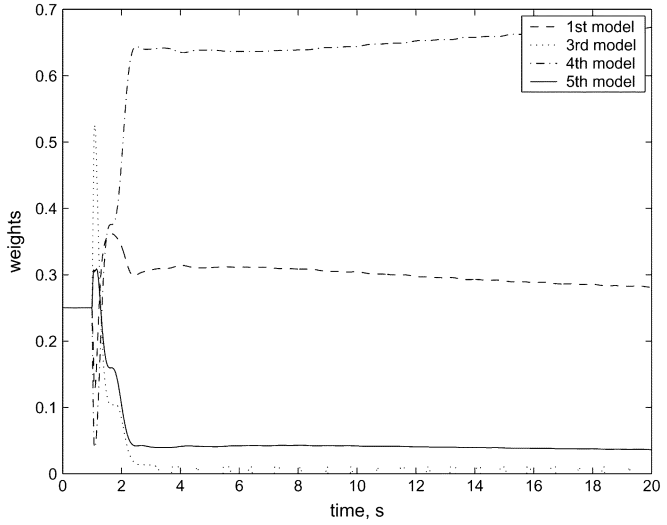

Fig. 11. Test case II. Variation of the weights corresponding to each model.

tificial cutoff $\beta_{\min}$ is kept to a small value of 0.001 to avoid retaining these unwanted models during subsequent recursive steps. If more blending is desired, both $\beta_{\min}$ and C_f can be adjusted accordingly, as illustrated in the previous section.

Fig. 8 depicts the dynamic behavior of the system in response to the disturbance described in Section VII-A. The displays show the relative angular separation between machines #G1, #G4, and #G3, #G2. Interarea oscillation involves a group of machines in one area swinging against a group in another area and is, therefore, mostly manifested in these particular relative angular differences. It can be seen that the lightly damped oscillations are settled in 10–12 s in the presence of the applied control scheme. Power flow between buses #10 and #9, shown in Fig. 9, also settles within the stipulated time-frame. The sharp fall in the magnitude of power flow, just after 1s, is due to the inception of the fault which gets cleared after 80 ms. Fig. 10 shows the resultant control action, which is dominated by the response of controller #2, due to its higher weight, as shown in Fig. 7. The simulation results illustrate that the MMAC scheme is able to identify the predominant postdisturbance dynamics and switch the proper controller without any prior knowledge about the specific operating condition by using online recursive calculation of model probabilities and associated weights.

B. Test Case II

The results of the time domain simulation for test case II are shown in Figs. 11–14. Contrary to the previous case, the linearized model (model #2) of the power system governing the postdisturbance dynamics and the corresponding controller (controller #2), was intentionally removed from the model bank. As a result, none of the model weights attains steady-state value of almost one, unlike the previous case, see Fig. 11. After a few recursive steps, during which the trend is not very clear, it can be seen that the dynamics are governed primarily by models #4, #1, and #5, in that order. The amount of blending can be adjusted by changing C_f, and/or $\beta_{\min}$. In this case, the value of C_f was chosen to be relatively low (0.01) as the chances of converging to a single model is less. Also, the magnitude of the artificial cutoff $\beta_{\min}$ was increased to 0.01 to retain even the least probable models. Fig. 12 exhibits the dynamic behavior of the system in response to the same disturbance mentioned in the previous

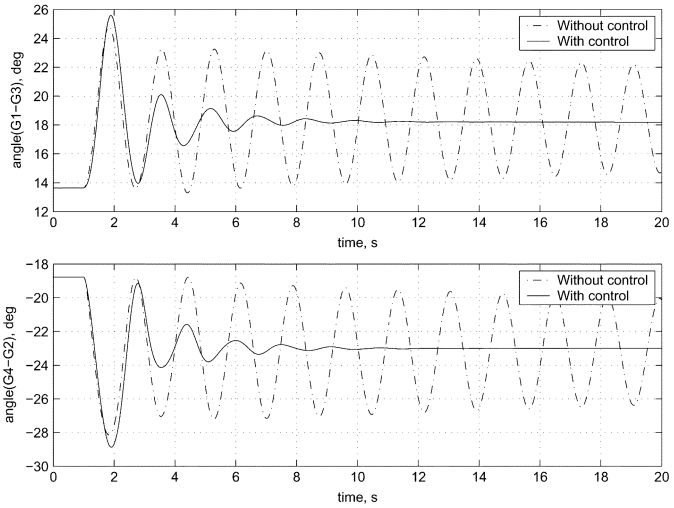

Fig. 12. Test case II. dynamic response of the system.

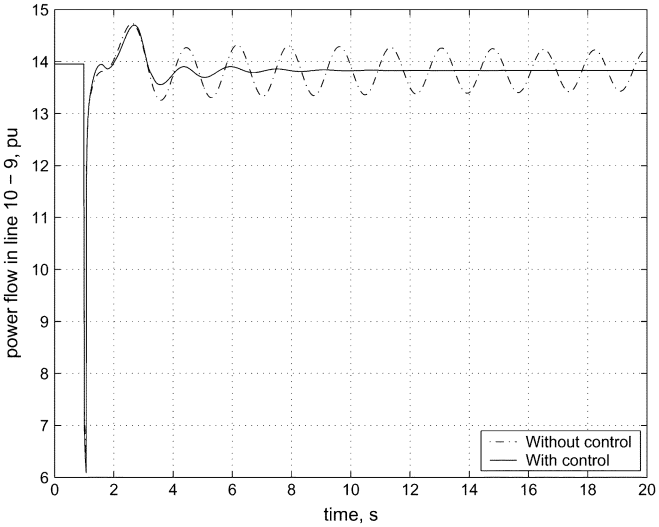

Fig. 13. Test case II. Power flow between buses #10 and #9.

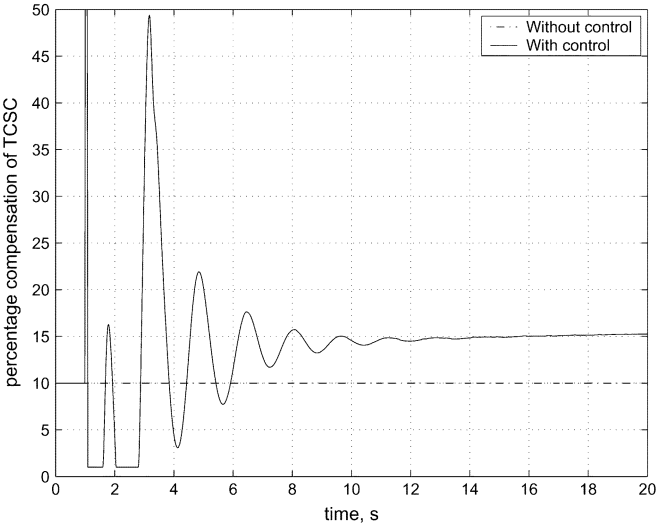

Fig. 14. Test case II. Response of the controller.

case. It can be seen that the lightly damped interarea oscillations are settled in 10–12 s. Power flow between buses #10 and #9, shown in Fig. 13, also settles within the specified time. Fig. 14 shows the resultant control action, which is dominated by the response of controllers #4, #1, and #5 due to their relatively higher weights, as shown in Fig. 11. The simulation results illustrate that, even though the actual model governing the response of the system after the disturbance is absent, the MMAC scheme is able to properly blend the control moves of the remaining controllers and still maintain reasonably similar performance. In fact, no noticeable deterioration can be observed in terms of performance in Fig. 12, when compared with Fig. 8. During the fault, the dynamics of the system is represented in a more realistic way by a combination of several models rather than a single model. This is particularly encouraging as it makes the MMAC scheme a reasonable candidate for application in large practical power systems, where the chances of convergence to a single model are remote, as described earlier.

X. Conclusion

In this paper, we have demonstrated the application of multiple-model adaptive control scheme for robust damping of interarea oscillations in power system using a TCSC. The lack of robustness of the conventional controllers under varying operating conditions is demonstrated underlying the motivation behind adopting such an adaptive strategy. A recursive Bayesian approach is used for computing the current probability of each model representing the actual system response and the results are used to determine the subsequent control move. The control output of each individual controller is assigned a weight based on the computed probability of each model and the resulting control action is the probability-weighted average of the control moves of individual controllers. The algorithm is shown to work satisfactorily for the study system under two different test cases where the model corresponding to the postdisturbance behavior is either present or not present in the model bank. When the model is present, the recursive Bayesian approach is able to identify the proper model within a few iterative steps and switch the appropriate controller accordingly. On the other hand, when the exact model is removed from the bank, the scheme performs proper blending of the remaining control moves to achieve reasonably similar performance as before. This highlights the potential applicability of the MMAC scheme for large practical power system where the dynamics are unlikely to be governed by a single model. Under such situation, the key to the success of the MMAC scheme is the rate of convergence of the probabilities, which in turn, is governed by the proper choice of convergence factor C_f and artificial cutoff $\beta_{\min}$. This paper provides a pattern of the variation of the computed weights for different values of C_f and $\beta_{\min}$ and attempts to set a tentative guideline for choosing them, depending on the situation. Currently, we are working on large practical power system models, where, even though the choice of these parameters is more involved depending on the degree of uncertainty, the basic guideline remains the same.

Acknowledgment

The authors gratefully acknowledge the ideas and suggestions received from S. Rakovic, Dr. A. C. Zolotas, Dr. I. M. Jaimoukha, and Dr. T. C. Green during this research.

References

[1] *CIGRE Special Publication 38.01.07*, Tech. Brochure 111, 1996.
[2] M. Klein, G. Rogers, and P. Kundur, "A fundamental study of inter-area oscillations in power systems," *IEEE Trans. Power Syst.*, vol. 6, pp. 914–921, Aug. 1991.
[3] P. Kundur, *Power System Stability and Control*. New York: McGraw-Hill, 1994.
[4] O. Malik, G. Hope, and V. Ramanujan, "Real time model reference adaptive control of synchronous machine excitation," in *Proc. IEEE PES Winter Meeting*, vol. 178, New York, 1976, pp. 297–304.
[5] N. Pahalawaththa, G. Hope, and O. Malik, "Multivariable self-tuning power system stabilizer simulation and implementation studies," *IEEE Trans. Energy Conversion*, vol. 6, pp. 310–316, June 1991.
[6] G. Bandyopadhaya and S. Prabhu, "A new approach to adaptive power system stabilizers," *Elec. Mach. Power Syst.*, vol. 14, pp. 111–125, 1988.
[7] D. Lainiotis, "Partitioning: A unifying framework for adaptive systems, II: Control," *Proc. IEEE*, vol. 64, pp. 1182–1198, Aug. 1976.
[8] M. Athans, D. Castanon, K.-P. Dunn, C. Greene, W. Lee, N. Sandell, and A. Willsky, "The stochastic control of the F-8C aircraft using a multiple-model adaptive control MMAC metnod—Part I: Equilibrium flight," *IEEE Trans. Automat. Contr.*, vol. AC-22, pp. 768–780, Oct. 1977.
[9] W. He, H. Kaufman, and R. Roy, "Multiple-model adaptive control procedure for blood pressure control," *IEEE Trans. Biomed. Eng.*, vol. BME-33, pp. 10–19, Jan. 1986.
[10] J. Martin, A. Schneider, and N. Smith, "Multiple-model adaptive control of blood pressure using sodium nitroprusside," *IEEE Trans. Biomed. Eng.*, vol. BME-34, pp. 603–611, Aug. 1987.
[11] R. Rao, B. Aufderheide, and B. Bequette, "Experimental studies on multiple-model predictive control for automated regulation of hemo-dynamic variables," *IEEE Trans. Biomed. Eng.*, vol. 50, pp. 277–288, Mar. 2003.
[12] P. Sauer and M. Pai, *Power System Dynamics and Stability*. Englewood Cliffs, NJ: Prentice-Hall, 1998.
[13] N. Hingorani and L. Gyugyi, *Understanding FACTS*. Piscataway, NJ: IEEE Press, 2000.
[14] M. Noroozian, L. Angquist, M. Gandhari, and G. Andersson, "Use of UPFC for optimal power flow control," *IEEE Trans. Power Delivery*, vol. 12, pp. 1629–1634, Oct. 1997.
[15] C. Yu, R. Roy, H. Kaufman, and B. Bequette, "Mutiple-model adaptive predictive control of mean arterial pressure and cardiac output," *IEEE Trans. Biomed. Eng.*, vol. 39, pp. 765–778, Aug. 1992.
[16] B. Kuo and F. Golnaraghi, *Automatic Control Systems*. New York: Wiley, 2003.

Balarko Chaudhuri (S'02) received the B.E.E. degree (Hons.) from Jadavpur University, Calcutta, India, in 2000 and the M.Tech. degree from the Indian Institute of Technology, Kanpur, India, in 2002. He is currently working toward the Ph.D. degree in the Control and Power Group, Imperial College London, London, U.K.

Rajat Majumder (S'04) received the B.E.E. (Hons.) from Jadavpur University, Calcutta, India and M.Sc.(Eng.) from the Indian Institute of Science, Bangalore, India in 2000 and 2003, respectively. He is currently working toward the Ph.D. degree in the control and power group at Imperial College London, London, U.K.

Bikash C. Pal (M'00–SM'02) received the B.E.E. (Hons.) degree from Jadavpur University, Calcutta, India, in 1990, the M.E. degree from and the Indian Institute of Science, Kanpur, India, in 1992, and the Ph.D. degree from Imperial College London, London, U.K., in 1999.

He is presently a Lecturer in the Department of Electrical and Electronic Engineering, Imperial College London. His research interest is in the area of power system dynamics and FACTS controllers.